https://doi.org/10.5194/egusphere-2025-4939
Preprint. Discussion started: 16 October 2025

On the Nationwide Variability of Low-Level Jets Prior to Warm-season Nocturnal Rainfall in China Revealed by Radar Wind Profilers

Ning Li[a,b], Jianping Guo[a,d*], Xiaoran Guo[a,d], Tianmeng Chen[a,d], Zhen Zhang[a], Na Tang[a], Yifei Wang[a], Honglong Yang[d], Yongguang Zheng[c]

[a] *State Key Laboratory of Severe Weather Meteorological Science and Technology & Specialized Meteorological Support Technology Research Center, Chinese Academy of Meteorological Sciences, Beijing 100081, China*

[b] *College of Earth and Planetary Sciences, University of Chinese Academy of Sciences, Beijing 100049, China*

[c] *National Meteorological Centre, Beijing 100081, China*

[d] *CMA Field Scientific Experiment Base for Low-Altitude Economy Meteorological Support of Unmanned Aviation in Guangdong-Hong Kong-Macao Greater Bay Area, Shenzhen 518108, China*

Correspondence to:

Dr./Prof. Jianping Guo (Email: jpguocams@gmail.com)

https://doi.org/10.5194/egusphere-2025-4939
Preprint. Discussion started: 16 October 2025

Abstract

Nocturnal rainfall initiation is closely linked to low-level jets (LLJs), but national-scale LLJ features over China—especially their evolution preceding warm-seasonal nocturnal rainfall—remain unknown due to scarce high-resolution vertical wind observations. Here, we reveal the multiscale responses of LLJs within 2 hours preceding the onset of nocturnal heavy rain (HR) and non-HR across four phases of rainy seasons in China during the warm season (April-October) of 2023–2024, utilizing data from a nationwide network of radar wind profilers (RWPs) in combination with surface observations and reanalysis data. Results show that nocturnal rainfall accounted for over 50% of warm-season rainfall, with 56% preceded by LLJs within 2 hours leading up to their onset. In monsoon regions, ~40% of nocturnal HR (LLJ_HR) were LLJ-associated and had higher heavy rainfall probability than non-LLJ_HR. Critically, these LLJ_HR events depended on rapid, coupled minute-scale dynamical intensification, typically occurring 30 to 120 minutes before rainfall initiation. Specifically, coherent changes in LLJ wind profiles, frequency, vertical wind shear, and pronounced evolution in jet height were observed, operating in synergy with substantial thermodynamic instability. This behavior stood in sharp contrast to LLJ_non-HR events, which were characterized by relatively stable, weakening, or declining LLJ evolution and an inadequate thermodynamic response. These findings demonstrate that a minute-scale 'rapid reorganization' of dynamic and thermodynamic conditions driven by swift evolution of the LLJ is essential for nocturnal HR, providing observational constraints for regional model parameterizations and nowcasting.

https://doi.org/10.5194/egusphere-2025-4939
Preprint. Discussion started: 16 October 2025

Short Summary

Nighttime rainfall often links to low-level jets (LLJs), but we lack clarity on nationwide LLJ features due to limited wind data. To address this, we used a nationwide radar wind profiler network to study LLJ changes 2 hours before rainfall, covering China's 2023–2024 rainy seasons. 56% nighttime rainfall had LLJs. The heavy rains linked to LLJs needed LLJs to strengthen quickly 30–120 minutes preceding rain. These findings show the importance of LLJ in nowcasting nighttime rainfall.

https://doi.org/10.5194/egusphere-2025-4939
Preprint. Discussion started: 16 October 2025

1. Introduction

Forecasting nocturnal heavy rainfall (HR) and associated severe convective weather remains a major challenge in hazardous weather prediction (Davis et al., 2003; Trier et al., 2006), owing to the complexity of triggering mechanisms, the scarcity of continuous high-resolution observations, and inaccuracies in model parameterizations (Carbone and Tuttle, 2008; Reif and Bluestein, 2017; Weckwerth et al., 2019; Zhao et al., 2025). Crucially, the low-level jet (LLJ) that exhibit a diurnal cycle with a maximum at night is widely recognized as a key contributor to nocturnal HR (Bonner 1968; Mitchell et al., 1995; Tuttle and Davis, 2006), as documented in regions or countries such as the Great Plains of the United States (Maddox, 1983; Higgins et al., 1997), Argentina (Marengo et al., 2004), India (Monaghan et al., 2010), North China Plain (Li et al., 2024).

The LLJs primarily originate from the inertial oscillations (IO) following the sudden decay of turbulence after sunset (Blackadar, 1957) and thermal imbalances induced baroclinicity over sloping terrain (Holton, 1967). Functioning as concentrated corridors for heat, moisture, and momentum transport, LLJs can modulate the diurnal oscillation in water vapor by IO (Rasmusson, 1967; Zhang et al., 2019) and enhance convective instability, particularly when elevated high-θ_e air encounters frontal boundaries (Trier et al., 2017). Also, strong low-level vertical wind shear (VWS) associated with LLJs necessarily benefits deep lifting (Maddox et al., 1979; Stensrud, 1996; Rasmussen and Houze, 2016). These mechanisms collectively provide essential thermodynamic and dynamic support for the initiation and organization of nocturnal convection, especially where LLJs force low-level ascent at jet termini or via positive vorticity advection left of the jet axis (Chen et al., 2017; Du and Chen, 2019; Xia and Zhao, 2009).

Furthermore, LLJs interact synergistically with other key factors to trigger HR, including terrain effects (Anthes et al., 1982; Pan and Chen, 2019; Huang et al., 2020), gravity waves (Weckwerth & Wakimoto, 1992), and mesoscale systems (Chen et al. 2010; Chen et al., 2017), among others. These interactions are highly sensitive to the prevailing synoptic and subsynoptic-scale environmental conditions (e.g., Hodges and Pu, 2019) and fine-scale structural of LLJs, including LLJ frequency, spatial redistribution, and particularly localized wind profile accelerations (Pitchford and London, 1962; Walters and Winkler, 2008; Du and Chen, 2019; Li et al., 2024). Understanding these intricate evolution features of LLJs is critical for improving the forecasting of nocturnal HR.

Despite advances facilitated by regional reanalysis (e.g., Doubler et al., 2015; Li et al., 2021), numerical modeling (e.g., Zhang and Meng, 2019), radiosonde observations (e.g., Whiteman et al., 1997; Yan et al., 2020), and emerging artificial intelligence techniques (e.g., Subrahmanyam et al., 2024) in understanding the climatology and physical mechanisms of LLJs and their role in HR forecasting, significant knowledge gaps remain. However, a critical shortcoming lies in the inability to capture minute-scale evolution of LLJs during the nocturnal pre-storm period. Conventional observing systems lack the spatiotemporal resolution required to resolve rapid changes in pre-storm environments (Weisman et al., 2015; Cao et at., 2025; Roots et al., 2025), thereby hindering systematic analysis of fine-scale structure of LLJs and their evolution within the critical 2-hour window preceding rainfall.

Moreover, the mechanisms and impacts of LLJs exhibit considerable variation across monsoon phases and geographic regions. As a classic monsoon climate region, China exhibits particularly prominent nocturnal rainfall contributions across major climate-sensitive areas (Yu et al., 2014),where LLJs play a crucial role in modulating primary rainfall belts (Sun, 1986; Chen et al., 2010; Wang et al., 2013; Horinouchi et al., 2019), such as those in Eastern China (Chen et al., 2017; Xue et al., 2018) and South China (Du et al., 2020; Bai et al., 2021; Fu et al., 2021). However, nationwide comparative studies examining LLJ precursor signals across different monsoon phases in China are still lacking.

Radar wind profilers (RWPs) can offer transformative potential by capturing minute-resolution wind profiles to reveal pre-rainfall dynamic precursors (Zamora et al., 1987; Du et al., 2012; Molod et al., 2019; Guo et al., 2023). For example, Gebauer

https://doi.org/10.5194/egusphere-2025-4939
Preprint. Discussion started: 16 October 2025

et al. (2018) demonstrated the capability of RWPs to elucidate how heterogeneous structures of LLJ trigger nocturnal convection in Great Plains; Based on a linear net of RWPs deployed across the North China Plain, Li et al. (2024) observed rapid intensification of MFC driven by a surge in LLJs profile within 30 min preceding nocturnal rainfall onset, highlighting the sensitivity of RWP to minute-scale perturbations of LLJs profiles.

Therefore, this study utilizes a nationwide network of RWPs to address the following two questions: 1) How do the vertical structure of LLJs and their minute-scale evolution within 0–2 hours preceding nocturnal rainfall vary across different rainy season phases? and 2) What are the systematic differences in LLJ dynamic-thermodynamic mechanisms between LLJ-influenced HR and non-HR events? The remainder of this paper is structured as follows: Section 2 details data and methodology, Section 3 presents comparative analyses of characteristics of rainfall and LLJs evolution, and Section 4 synthesizes key conclusions.

2. Data and Methodology

2.1 Radar wind profiler measurements

The RWP observations collected from 31 stations across China (Fig.1) from April to October in 2023-2024 were analyzed in this study, which can provide wind speed and direction with a vertical resolution of 120 m and an interval of 6 minutes (Liu et al., 2019). To reduce the potential influence of poor data quality, RWP data underwent strict quality control following procedures proposed by Wei et al. (2014) and Miao et al. (2018). Firstly, observations recorded during rainfall periods were eliminated. Secondly, for each profile, if more than 40% of the data points below 3 km above ground level (AGL) were outliers or missing, that entire profile was discarded. Next, within each profile below 3 km AGL, missing values and significant outliers that defined as values exceeding 2.5 standard deviations from the mean were removed. Finally, discontinuous, or missing data points were estimated using linear interpolation.

Following this quality control process, 109,400 wind profiles were discarded and a total of 2,606,042 profiles across China were available for analysis during the study period.

2.2 Miscellaneous meteorological data

In addition, 1-min rainfall measurements were directly acquired from the rain gauge measurements at 2160 national weather stations across China to identify rainfall events. Rainfall amounts were accumulated over 6-min intervals to ensure temporal alignment with the RWP measurements. Ground-based meteorological variables are measured at 1-min intervals from national weather stations, including 2-m air temperature, relative humidity, and surface pressure. All ground-based data have undergone rigorous quality control and are publicly available by the China Meteorological Administration (CMA).

Furthermore, to diagnose large-scale circulation patterns and environmental conditions preceding nocturnal rainfall influenced by LLJs, this study utilized meteorological variables derived from the fifth generation of the European Centre for Medium-Range Weather Forecasts atmospheric reanalysis (ERA5) of the global climate (Hersbach et al., 2020). The ERA5 data features a horizontal resolution of 0.25°×0.25° across 37 vertical pressure levels and hourly temporal resolution. Unless otherwise specified, all datasets cover the study period of April to October in 2023–2024.

2.3 Identification of nocturnal rainfall events

Firstly, days with typhoon activity were excluded. To minimize the impact of rainfall on RWP measurements, a minimum dry interval of 2 hours was required between consecutive rainfall events. Following the methodology of Li et al. (2024), a rainfall occurrence was defined when the total accumulated rainfall which was measured by all rain gauges within a 25-km radius of each RWP station exceeded 0.1 mm. Accounting for rainfall intermittency, a valid rainfall event required at least two subsequent occurrences within 30 min following initial detection. Any isolated initial occurrence not meeting this criterion was discarded.

https://doi.org/10.5194/egusphere-2025-4939
Preprint. Discussion started: 16 October 2025

Nocturnal rainfall events were defined as those occurring between 2000 and 0800 Local Standard Time (LST). Based on operational classifications from the National Water Resources Bureau and CMA, the rainy season was categorized into four consecutive phases: (1) the South China Pre-summer Rainy Season (April 1 to June 8, 2023 and April 1 to June 9, 2024), (2) the Meiyu Season (June 9 to July 14, 2023 and June 10 to July 21, 2024), (3) the North China Rainy Season (July 22 to August 31, 2023 and July 15 to August 31, 2024), and (4) the West China Autumn Rainy Season (September 1 to October 31 for both 2023 and 2024), These phases are subsequently designated as Phase 1 to Phase 4 throughout this study. Four regions of interest (ROIs) were subsequently selected for detailed analysis (see Table 1).

Further screening identified nocturnal HR events where the mean 6-min rainfall intensity exceeded the 75th percentile of all rainfall events at each station. Statistical analysis revealed 3,155 nocturnal rainfall events during the 2023–2024 warm seasons (within the 31 red circles shown in Fig.1). Event counts per rainy season phase were 1,109, 689, 652, and 705 respectively, with 841 events classified as nocturnal HR events.

2.4 Identification of LLJs and associated rainfall event

To ensure identified LLJs exhibit significant vertical wind shear characteristic of jet-like profiles, the following criteria are adopted: (1) a maximum horizontal wind speed exceeding10 m s^{-1} in the lowest 3 km AGL, and (2) a wind speed reduction of at least 3 m s^{-1} from the maximum to minimum below 3 km AGL, or to 3 km AGL if no minimum exists (Bonner, 1968; Whiteman et al., 1997; Du et al., 2014; Yan et al., 2020). These deliberately conservative wind speed thresholds maximize LLJ sample size for enhanced statistical robustness. The strength of LLJ or jet nose is defined as the maximum wind speed along the entire profile. The LLJ core height is defined as the altitude of the wind speed maximum during LLJ occurrences. Correspondingly, the LLJ direction is determined by the wind direction at the height of the LLJ.

We define rainfall events where LLJ occurs at least twice within 2 hours before rainfall as an LLJ event. And HR events influenced by LLJs (LLJ_HR events), HR

https://doi.org/10.5194/egusphere-2025-4939
Preprint. Discussion started: 16 October 2025

events without LLJ influence (non-LLJ_HR events), and non-HR events affected by LLJ (LLJ_non-HR events) are further distinguished.

3. Results and discussion

3.1 General characteristics of nocturnal rainfall and LLJs

Firstly, we characterized the spatiotemporal patterns of rainfall and LLJs observed nationwide during the 2023-2024 warm season. Nationally, nocturnal rainfall accounted for 51.6% of total warm-season rainfall (Fig. 2g), with pronounced concentrations over North, East, and Southwest China. In contrast, the pronounced daytime rainfall dominance in South China may arise from sea-breeze-front convective systems triggered by afternoon land-sea thermal contrasts and rapid destabilization of the local boundary layer. The frequency of nocturnal rainfall (52.5%) notably exceeded that in the daytime (47.5%) at the national scale, with the highest values occurring over southwestern and eastern regions (Fig. 2h). While the North China displayed distinct characteristics of low-frequency but high-intensity nocturnal rainfall. Although mean nocturnal rainfall intensity was generally lower, the probability of HR was higher at night than during the day, particularly across western China, North China, and northeastern China (Fig. 2i).

Figure 3 displayed key attributes of LLJs detected at all 31 RWPs across China using Section 2 criteria. Compared to daytime, the occurrence frequency of nocturnal LLJs increased significantly by nearly 18%, with the most pronounced enhancement observed particularly over northern and eastern regions where nocturnal rainfall is more intense. Nocturnal LLJs exhibited stronger strength of core and highly occurrences below 1 km AGL, reflecting enhanced nocturnal LLJs within the boundary layer vertically. This vertical restructuring likely responds to nocturnal surface cooling and resultant low-level wind-field modifications. The dominant wind direction shifted to southerly or southwesterly flows at night across most regions, potentially driven by thermal contrasts within the monsoon circulation pattern and topographic forcing.

Statistical analysis revealed substantial linkage between LLJs and nocturnal rainfall. Specifically, 56% of nocturnal rainfall events across China were preceded by the presence of LLJs within 2 hours. Consequently, nocturnal rainfall influenced by LLJs represents a major component of warm-season rainfall in China. And this relationship was modulated by the seasonal migration of the western Pacific subtropical high (WPSH), which drove corresponding shifts in HR belts that closely synchronized with the spatiotemporal evolution of LLJ activity. The proportion of nocturnal rainfall events associated with LLJs during the four rainy season phases reached 60.4%, 56.3%, 49.4%, and 54.9%, respectively (Fig. 4a). Among 841 identified nocturnal HR events, the percentages classified as LLJ_HR events were 47.2%, 43.6%, 33.9%, and 45.5% from Phase 1 to Phase 4. For non-HR events, LLJ_non-HR events accounted for approximately 37.8%. These statistics collectively demonstrate the crucial role of LLJs in initiating and modulating nocturnal rainfall across China.

Spatial analysis of rainfall intensity further revealed that LLJ_HR events consistently produced heavier rainfall than non-LLJ_HR events, particularly within the four ROIs identified in each phase (red boxes in Fig. 5). Therefore, a total of 142, 118, 63, and 59 nocturnal HR events were identified in these ROIs during from Phase 1 to Phase 4 (Fig. 4b). From the LLJs perspective, nearly 31.1% of LLJ events were classified as HR events across phases relative to LLJ_non-HR events, which suggests the presences of LLJs do not inherently increase the occurrence of HR. From the HR perspective, nearly 45.0% of HR events were associated with LLJs within 2 hours before occurred relative to non-LLJ_HR events (see the pie charts in Fig. 6). And the highest proportion of LLJ_HR events occurred over ROI-2 during Phase 2, while the lowest occurred in ROI-4 during Phase 4. In general, while nearly half of HR events involved LLJs, merely 30% of LLJ events produced HR, indicating LLJs are necessary but insufficient for HR.

Furthermore, probability distributions of rainfall intensity (Fig. 6) indicated that LLJ_HR events generally produced heavier rainfall at the national scale compared to non-LLJ_HR events, though the differences were less pronounced during Phases 2 and 4. Within the key regions, both event types showed higher probabilities of HR than the

https://doi.org/10.5194/egusphere-2025-4939
Preprint. Discussion started: 16 October 2025

national average, particularly for LLJ_HR events. LLJ_HR events in ROI-1 and ROI-2 demonstrated significantly higher probabilities of extreme rainfall (≥ 2 mm/6 min), while those in ROI-4 during Phase 4 favored intensities near 0.5 and 2.8 mm/6 min. Notably, although ROI-3 in Phase 3 exhibited a relatively high proportion of LLJ_HR events, their probability of producing heavier rainfall was lower than for non-LLJ_HR events, suggesting that LLJs may not represent the dominant mechanism for extreme rainfall in this particular region and season.

3.2 Minute-scale evolution of LLJs preceding nocturnal heavy and non-heavy rainfall

Although previous analyses have established the importance of LLJs in HR events, it is noteworthy that approximately 70% of LLJ occurrences were not accompanied by concurrent HR (i.e., LLJ_non-HR events). To elucidate the contrasting precursor characteristics of LLJs that lead to nocturnal rainfall of differing intensities, this section examines fine-scale vertical structure and continuous evolution of LLJs within 2 hours preceding both LLJ_HR and LLJ_non-HR events during four phases in their respective ROIs. The results reveal distinct spatiotemporal variations in vertical structure and evolutionary patterns of LLJs.

During Phase1 in ROI-1, LLJ_HR events exhibited a significant increase in frequency starting 108 min before rainfall onset, reaching secondary peaks at –84 min and –60 min and culminating in maximum frequency immediately preceding rainfall (Fig. 7a). These LLJs featured a bimodal vertical distribution with frequent occurrence layers at 0.5–1 km and 1.5–2 km AGL. Wind profiles showed that LLJs strength maximized at 48 min preceding rainfall accompanied by a slight downward extension, followed by a modest weakening (Fig. 8a). In contrast, LLJ_non-HR events exhibited lower overall frequency predominantly below 1 km AGL, although they showed gradual frequency increases from -48 min alongside strengthening winds and rising jet heights (Figs. 7e and 8e).

However, both event types exhibited notably high frequencies and intensities of LLJs over ROI-2 during Phase 2. For LLJ_HR events, the total frequency and height

https://doi.org/10.5194/egusphere-2025-4939
Preprint. Discussion started: 16 October 2025

of LLJ occurrence initially declined followed by a rise. At –120 min, the frequency of LLJs peaked and strength of jet profile reached a maximum (exceeding 12 m s⁻¹). These values then rapidly declined to a minimum at -84 min, concurrent with the jet height descending from 1.5–2 km to below 1 km AGL. Then frequency of LLJs subsequently increased with gradual height recovery, reaching a secondary peak at –48 min while intensity of jet nose stabilized near 11 m s⁻¹. In comparison, LLJ_non-HR events maintained consistent LLJs strength (near 11.8 m s⁻¹) and a preferred height range of 1–2 km AGL (Fig. 8f). And LLJs frequency exhibited gradual changes, culminating in a single peak 36 min before rainfall, followed by a rapid decrease (Fig. 7f).

During Phase 3 in ROI-3, LLJ_HR events exhibited a bimodal temporal distribution in LLJ frequency, with distinct peaks occurring at –96 min and –48 min prior to rainfall (Fig. 7c). The dominant LLJ height was centered between 1–1.5 km AGL. Beginning approximately 30 min before rainfall onset, a discernible descent of the jet core was observed, accompanied by accelerated intensification of the wind profile, which reached its maximum strength by –48 min (Fig. 8c). This rapid vertical restructuring of LLJ is likely a key factor influencing HR occurrence. However, markedly weaker wind profiles (near 9 m s⁻¹) potentially explained the lower probability of heavier rainfall in LLJ_HR events over ROI-3 during Phase 3 relative to other region and phases. Conversely, LLJ_non-HR events were characterized by lower LLJs frequency and a more uniform height distribution (Fig. 7g).

During Phase 4 in ROI-4, LLJ_HR events showed a rapid frequency increase from 48 min prior to rainfall. The LLJs were concentrated between 0.5–1.5 km AGL, and the intensity of wind profile intensified progressively, with average maximum peaking near 13 m s⁻¹ just before rainfall onset (Fig. 8d). Conversely, LLJ_non-HR events peaked earlier at –84 min in both frequency and intensity of LLJs, followed by general attenuation (Fig. 7h). By -48 min, wind profiles stabilized into a double-core structure maintaining around 10 m s⁻¹, with distinct jet cores near 0.8 km and 1.7 km AGL (Fig. 8h).

Furthermore, probability distributions of LLJ strength and height within 2 hours preceding rainfall were compared across key regions (Fig. 9). During Phase 1 in ROI-

https://doi.org/10.5194/egusphere-2025-4939
Preprint. Discussion started: 16 October 2025

1, the strength of LLJs in LLJ_HR events was notably stronger by 2–3 m s⁻¹ than that in LLJ_non-HR events (Fig. 9a). Height distributions showed distinct bimodal peaks near 0.9 km and 1.75 km AGL (Fig. 9e), consistent with previously documented double LLJs influences (Du and Chen, 2019). And average LLJs height was generally higher in LLJ_HR events. During Phase 2 in ROI-2, LLJ_HR events showed higher probabilities of strong LLJs (17–28 m s⁻¹) compared to the dominant 13 m s⁻¹ intensity in LLJ_non-HR events (Fig. 9b). Influenced by large-scale circulation patterns, both event types featured LLJs centered near 1.5 km AGL (Fig. 9f), though LLJ_HR events developed a secondary maximum near 0.8 km AGL due to pre-rainfall descent of the jet core (Fig. 7b). Contrastingly, Figure 9c shows that LLJ_HR events were associated with weaker jet strengths (around 11 m s⁻¹) compared to LLJ_non-HR events (14–23 m s⁻¹) in ROI-3 during Phase 3, suggesting that strong LLJs don't necessarily induce HR here. The height of LLJ in LLJ_HR events mainly concentrated near 1.2 km AGL, whereas in LLJ_non-HR events, it was more uniformly distributed between 0–3 km AGL with a higher probability above 1.7 km (Fig. 9g). For Phase 4 in ROI-4, LLJs strength peaked near 15 m s⁻¹ in both event types, but LLJ_HR events featured stronger jets reaching 25-30 m s⁻¹ (Fig. 9d). And LLJs height in both events peaked predominantly at 0.8 km AGL, with secondary peaks at 1.5 km for LLJ_HR and 2.0 km AGL for LLJ_non-HR events (Fig. 9h).

In summary, distinct temporal evolution patterns in frequency, occurrence height, and wind profile intensity of LLJs preceding LLJ_HR events were observed across key regions during each phase. Except for ROI-3 during Phase 3, LLJ_HR events exhibited significantly higher probabilities of stronger jets, most notably in ROI-2 during Phase2. LLJs height were generally lower in LLJ_HR events, except in ROI-1 during Phase1. These findings highlight the role of fine-scale LLJ structures and their rapid vertical reorganization in modulating nocturnal rainfall intensity, offering valuable insights for improving regional nocturnal HR forecasting.

https://doi.org/10.5194/egusphere-2025-4939
Preprint. Discussion started: 16 October 2025

3.3 Thermodynamic evolution associated with LLJs preceding nocturnal heavy and non-heavy Rainfall

The preceding section 3.2 has clarified that the fine-scale dynamic characteristics of LLJs—including their temporal evolution, vertical structure, and intensity variations—play a pivotal role in modulating nocturnal rainfall intensity across different key regions and rainy season phases. However, the influence of LLJs on rainfall generation and intensification rarely operates in isolation; instead, it depends strongly on the accompanying large-scale thermodynamic environment, which provides the necessary moisture supply and convective instability to sustain or amplify heavy rainfall. Thus, to fully unravel the mechanisms underlying the distinction between LLJ_HR and LLJ_non-HR events, it is essential to complement the dynamic analysis with an in-depth examination of the thermodynamic conditions associated with LLJs in the 1-hour preceding nocturnal rainfall.

Further analysis of large-scale thermodynamic conditions at 1-hour preceding rainfall (Figs. 10 and 11) reveals consistently stronger thermal instability for LLJ_HR versus LLJ_non-HR events, accompanied by stronger MFC within key regions during each rainy season.

During Phase 1 in ROI-1, thermodynamic conditions were comparable between event types. Southwesterly LLJs transported warm-moist air masses from the South China Sea and Bay of Bengal, forming a pronounced warm-humid tongue. Coupled with MFC centers developing north of the jet axis, this configuration facilitated nocturnal rainfall development. During Phase 2 in ROI-2, although warm-moist airflow prevailed northwest of the subtropical high in both event types, LLJ_HR events exhibited more favorable thermodynamic conditions: mean θ_e was approximately 2 K higher than in LLJ_non-HR events, with a high-θ_e center reaching 358 K, alongside stronger LLJ cores (>1.2 m s^{-1} difference). Through baroclinic instability and LLJ dynamic forcing, strong MFC centers formed along the left side of the jet axis, ultimately triggering HR. During Phase 3 in ROI-3, LLJ_HR events were characterized by enhanced southwesterly moisture transport interacting with cold air advection from westerly troughs. Superimposed with topographic forcing from the Taihang Mountains, this resulted in MFC intensities south of Beijing nearly 30×10^{-5} km $m^{-2}s^{-1}$ than those in LLJ_non-HR events, thereby driving nocturnal HR. Thermodynamic contrasts were most pronounced during Phase 4 in ROI-4. Unlike LLJ_non-HR events characterized by southwestward-extending cold highs, LLJ_HR events developed deep high-θ_e centers (>360 K) over the southeastern Tibetan Plateau, supplying abundant moisture and convective instability. Concurrently, stronger anticyclonic circulation (consistent with enhanced LLJ winds in Fig. 8d) drove cold air intrusion into ROI-4. This cold airflow converged with warm-moist plateau currents over the Sichuan Basin, synergizing with orographic forcing to generate a strong MFC center on the eastern lee slope of plateau to promote nocturnal HR in ROI-4.

To elucidate the rapid processes leading to occurrence of rainfall, the minute-scale evolution of key thermodynamic and dynamic parameters was further analyzed (Fig. 12), including surface θ_e, LLJ index (defined as the ratio of maximum wind speed below 3 km to the height where wind first exceeds 10 m s^{-1}) and VWS (calculated as the wind speed difference between the surface and jet height divided by the jet height).

Figure 12a shows that during Phase 1 in ROI-1, although large-scale environments were similar between event types (LLJ_HR and LLJ_non-HR), the rapid, minute-scale co-intensification of thermodynamic and dynamic process prior to rainfall onset governs the resulting rainfall intensity. LLJ_HR events exhibited abrupt thermodynamic enhancement at 90 min preceding the onset of rainfall, with surface θ_e and VWS surging approximately1.5 K and 0.5 s^{-1}respectively. Concurrently, the LLJ index surged by 0.03 and VWS peaked sharply at -60 min, signaling LLJs intensification and core descent (Figs. 7a, 8a). This coordinated intensification suggests a tightly coupled process in which low-level warming and moistening reinforced wind acceleration, thereby enhancing shear and promoting deeper lifting conducive to HR. In contrast, LLJ_non-HR events showed weaker increases and a declining LLJ index (by about 0.015) alongside rising jet cores, reducing low-level shear and convergence efficiency, thereby diminishing overall rainfall intensity.

During Phase 2 in ROI-2, LLJ_HR events showed concurrent peaks in dynamic parameters (LLJ index, strength and VWS) coupled with high θ_e (348.3K) at -120 min (Fig. 12b). At -84 min, a critical rapid descent of jet core height below 1 km AGL coincided with surface warming and a LLJ index maximum. This change likely enhanced boundary-layer convergence by bringing stronger winds into closer proximity to the surface, effectively steepening VWS and facilitating deeper convective initiation. The timing of this rapid evolution suggests a transient optimal window for nocturnal rainfall triggering that is characteristic of LLJ_HR events in ROI-2. Subsequently, the LLJ index declined sharply and a rapid surface cooling initiates beginning 60 min prior to HR likely resulted from the outflow of cold pool outflow associated with alternation of convective systems in the Mei-Yu front cloud system (Zhang et al., 2023). The combination of the cold air and the strong southwestly LLJs may have further enhanced uplift and promoted rainfall (Luo et al., 2014). For LLJ_non-HR events, weaker thermodynamic support and diminished dynamic forcing with consistently lower LLJ indices (ΔI≈0.015) within 60 min preceding rainfall resulted in insufficient lift to sustain HR. These contrasting features underscored the importance of thermal-dynamic synergy influenced by LLJs evolution in triggering HR.

During Phase 3 in ROI-3, LLJ_HR events featured prominent thermal compensation (surface $\Delta\theta_e$ > 1K, 850hPa $\Delta\theta_e$> 2K versus non-HR events) despite weaker dynamics compared to other phases (Fig. 12c). The LLJ index progressively increased while VWS peaked synchronously with LLJ frequency. Within 30 min preceding rainfall, substantial intensification of VWS by about 1.5 m s^{-1} occurred driven by a rapid acceleration in the LLJ wind profile. This co-evolution with rapid surface warming (increase of 0.25 K) released convective instability, enhancing boundary-layer convergence (Fig. 10) and explaining the stronger MFC observed. Nevertheless, the overall weaker dynamical conditions likely limited the depth and organization of convection, explaining the reduced probability of heavier rainfall compared to other phases.

And LLJ_HR events showed explosive dynamic intensification from 48 min preceding rainfall in ROI-4 during Phase 4. with VWS surging 0.9 s^{-1} and LLJ index

https://doi.org/10.5194/egusphere-2025-4939
Preprint. Discussion started: 16 October 2025

0.025 (Fig. 12d). This rapid strengthening of the jet occurred concurrently with a gradual rise in θ_e (>346 K), enhancing low-level moist static energy and supporting vigorous uplift along the windward slopes of the Sichuan Basin. The synergistic coupling between dynamic forcing and thermodynamic persistence underscores the critical role of minute-scale jet intensification as a precursor to nocturnal HR under favorably pre-conditioned environments in ROI-4. For LLJ_non-HR events, VWS and surface θ_e reached their peaks almost simultaneously at 84 min before rainfall followed by gradual decline. The premature peak and subsequent decay in both dynamic and thermodynamic fields resulted in a lack of sustained forcing during the critical pre-convective period. And these events exhibited weaker changes of dynamics with marginal temporal evolution (VWS < Δ0.45 s^{-1}, ΔI < 0.02), reflecting an absence of the coordinated intensification necessary to initiate and sustain HR.

Overall, these results adequately showcase the sensitivity of regional HR to the fine-scale structural evolution of LLJs and their coupling with thermodynamic environments.

4. Summary and concluding remarks

There exists a critical gap in the observation of minute-scale LLJ evolution prior to nocturnal rainfall. To fill this knowledge gap, this study presents the first nationwide analysis of continuous LLJ dynamics using observations from 31 RWPs across China during the warm seasons (April–October) of 2023–2024. We examined vertically resolved differences in LLJ behavior within 2 hours preceding nocturnal HR and non-HR events throughout four distinct phases of the rainy season and investigated associated thermodynamic regulatory mechanisms.

At the national scale, nocturnal rainfall accounted for nearly half of the total warm-season precipitation, with 56% of these nocturnal events exhibiting LLJ influence within the preceding 2 hours. Furthermore, nocturnal HR events in ROIs during the four different phases of rainy season were identified. Statistical results revealed that approximately 45.0% of HR events were associated with LLJs. which exhibited a

https://doi.org/10.5194/egusphere-2025-4939
Preprint. Discussion started: 16 October 2025

higher probability of producing heavier rainfall than non-LLJ_HR events, underscoring the strong linkage between LLJs and nocturnal HR.

Pronounced differences and varying lead times were observed in vertically resolved evolution of LLJs and their thermodynamic environments when comparing LLJ_HR and LLJ_non-HR events. During Phase 1 in ROI-1, LLJ_HR events were marked by a sharp rise in LLJ frequency beginning 108 min before rainfall, accompanied by abrupt thermodynamic intensification ($\Delta\theta_e \approx 1.5$K, ΔVWS≈ 0.5 s^{-1}) from -90 min. In contrast, LLJ_non-HR events exhibited weaker and more stable thermo-dynamic conditions. During Phase 2 in ROI-2, LLJ_HR events were preceded by initially strong jets (>12 m s^{-1}) and elevated surface θ_e (~348.3 K), followed by a rapid descent of the LLJ core below 1 km AGL at -84 min, leading to a peak in the LLJ index. While LLJ_non-HR events were characterized by a stable jet core but declining dynamic indices and frequency within the final 60 min before rainfall. During Phase 3 in ROI-3, LLJ_HR events exhibited higher LLJ frequency and an increasing LLJ index, culminating in rapid wind profile restructuring within 30 min before rainfall, all under significantly more unstable thermal conditions (surface $\Delta\theta_e$ > 1 K) compared to non-HR events. During Phase 4 in ROI-4, LLJ_HR events were driven by favorable thermodynamic environments and minute-scale dynamical changes. A surge in jet frequency at -48 min triggered abrupt increases in VWS (≈0.9 s^{-1}) and the LLJ index (≈0.025) accompanied with high θ_e air, enhancing strong MFC over the southeastern plateau. By contrast, LLJ_non-HR events lacked adequate thermal forcing, and LLJ intensity, frequency, and dynamical parameters showed a consistent declining trend.

Crucially, A key finding is that nocturnal LLJ_HR events universally require rapid, coupled minute-scale dynamical intensification occurring 30-120 min preceding rainfall onset, acting in synergy with thermodynamic instability. LLJ_non-HR events consistently displayed insufficient dynamic-thermodynamic coupling, reflected in stable or declining LLJ parameters. This underscores that the intensity and timing of nocturnal rainfall are ultimately regulated by regionally specific thermo-dynamic interactions modulated by the evolution of fine vertical structure of the LLJ.

https://doi.org/10.5194/egusphere-2025-4939
Preprint. Discussion started: 16 October 2025

This study establishes distinct dynamic-rainfall linkages associated with LLJs across different warm-season rainy periods in China. Future research should: (1) expand multi-source observations to establish dynamic thresholds for early forecasting systems of nocturnal rainfall, and (2) develop quantitative frameworks relating LLJ structural evolution to rainfall intensity, offering theoretical support for optimizing physical processes in LLJ parameterization schemes within high-resolution numerical models. Additionally, the physical mechanisms governing evolution of LLJs height or strength immediately preceding rainfall onset require further investigation.

Data Availability

The LLJs retrieved from the RWP network can be acquired from https://doi.org/10.5281/zenodo.17176759 (Li and Guo, 2025). The data from the weather station are obtained from the China Meteorological Data Service Centre at https://data.cma.cn/en, and the original ERA5 reanalysis data used here are available from the ECMWF in Hersbach et al. (2020).

Acknowledgments

This work was supported by the National Natural Science Foundation of China under Grants of 42325501 and 42105090, and by the National Key Research and Development Program of China under grant 2024YFC3013001. Last but not least, we appreciated tremendously the constructive comments and suggestions made by the anonymous reviewers that significantly improved the quality of our manuscript.

Author Contributions

The study was completed with close cooperation between all authors. JG designed the research framework; NL performed the analysis and drafted the original manuscript with contribution from JG; JG, XG, ZZ, YZ. JG, NT and YW helped revise the manuscript.

Completing interests

The authors declare that they have no conflict of interest.

https://doi.org/10.5194/egusphere-2025-4939
Preprint. Discussion started: 16 October 2025

References

Anthes, R. A., Kuo, Y. H., Benjamin, S. G., and Li, Y. F: The evolution of the mesoscale environment of severe local storms: Preliminary modeling results, Mon. Weather Rev., 110(9), 1187-1213, doi:10.1175/1520-0493(1982)110,1187: TEOTME.2.0.CO;2, 1982.

Bai, L., Chen, G., Huang, Y., and Meng, Z.: Convection initiation at a coastal rainfall hotspot in South China: Synoptic patterns and orographic effects, J. Geophys. Res. Atmos., 126(24), e2021JD034642, doi: 10.1029/2021JD034642, 2021.

Blackadar, A. K.: Boundary layer wind maxima and their significance for the growth of nocturnal inversions, Bull. Am. Meteorol. Soc., 38(5), 283-290, doi:10.1175/1520-0477-38.5.283, 1957.

Bonner, W. D.: Climatology of the low-level jet, Mon. Weather Rev., 96(12), 833-850. doi:10.1175/1520-0493(1968) 096<0833:COTLLJ>2.0.CO;2, 1968.

Cao, Q., J. Guo, C. Xue, Z. Li, H. Xu, N. Li, Y. Sun, Z. Zhang, Y. Wang, J. Chen, Y. Zhou, and T. Chen: Divergent Sounding-derived Precursor Pathways Enable Discrimination of Dry versus Wet Severe Convective Winds. Geophysical Research Letters, 52, e2025GL117491. https://doi.org/10.1029/2025GL117491, 2025.

Carbone, R. E., and Tuttle, J. D.: Rainfall occurrence in the US warm season: The diurnal cycle, J. Clim., 21(16), 4132-4146, doi:10.1175/2008JCLI2275.1, 2008.

Chen, G., Sha, W., Iwasaki, T., and Wen, Z.: Diurnal Cycle of a Heavy Rainfall Corridor over East Asia, Mon. Weather Rev., 145(8), 3365-3389, doi:10.1175/mwr-d-16-0423.1, 2017.

Chen, H., Zhou, T., Neale, R. B., Wu, X., and Zhang, G. J.: Performance of the new NCAR CAM3. 5 in East Asian summer monsoon simulations: Sensitivity to modifications of the convection scheme, J. Clim., 23(13), 3657-3675, doi:10.1175/2010JCLI3022.1, 2010.

Chen, Y. L., and Li, J.: Large-scale conditions favorable for the development of heavy rainfall during TAMEX IOP 3, Mon. Weather Rev., 123(10), 2978-3002, 1995.

https://doi.org/10.5194/egusphere-2025-4939
Preprint. Discussion started: 16 October 2025

Davis, C. A., Maning, W. K., Carbone, R., Trier, S., and Tuttle, J.: Coherence of warm-season continental rainfall in numerical weather prediction models, Mon. Weather Rev., 131, 2667-2679, doi:10.1175/1520-0493(2003)131<2667:COWCRI>2.0.CO;2, 2003.

Dong, F., Zhi, X., Zhang, L., and Ye, C.: Diurnal variations of coastal boundary layer jets over the northern South China Sea and their impacts on diurnal cycle of rainfall over southern China during the early-summer rainy season, Mon. Weather Rev., 149(10), 3341-3363, doi:10.1175/MWR-D-20-0292.1, 2021.

Doubler, D. L., Winkler, J. A., Bian, X., Walters, C. K., and Zhong, S.: An NARR-derived climatology of southerly and northerly low-level jets over North America and coastal environs, J. Appl. Meteorol. Climatol., 54(7), 1596-1619, doi:10.1175/JAMC-D-14-0311.1, 2015.

Du, Y., and Chen, G.: Heavy Rainfall Associated with Double Low-Level Jets over Southern China. Part II: Convection Initiation, Mon. Weather Rev., 147(2), 543-565, doi:10.1175/mwr-d-18-0102.1, 2019.

Du, Y., Chen, G., Han, B., Bai, L., and Li, M.: Convection initiation and growth at the coast of South China. Part II: Effects of the terrain, coastline, and cold pools, Mon. Weather Rev., 148(9), 3871-3892, doi:10.1175/MWR-D-20-0090.1, 2020.

Du, Y., Zhang, Q., Ying, Y., and Yang, Y.: (2012). Characteristics of low-level jets in Shanghai during the 2008-2009 warm seasons as inferred from wind profiler radar data, J. Meteorol. Soc. Jpn. Ser. II, 90(6), 891-903, doi:10.2151/jmsj.2012-603, 2012.

Gebauer, J. G., Shapiro, A., Fedorovich, E., and Klein, P.: (2018). Convection Initiation Caused by Heterogeneous Low-Level Jets over the Great Plains, Mon. Weather Rev., 146(8), 2615-2637, doi:10.1175/mwr-d-18-0002.1, 2018.

Guo, J., Liu, B., Gong, W., Shi, L., Zhang, Y., Ma, Y., Zhang, J., Chen, T., Bai, K., Stoffelen, A., de Leeuw, G., and Xu, X.: Technical note: First comparison of wind observations from ESA's satellite mission Aeolus and ground-based radar wind profiler network of China, Atmos. Chem. Phys., 21, 2945-2958, doi: 10.5194/acp-

21-2945-2021, 2021 (data available at: https://data.cma.cn, last access: 11 January 2024).

Guo, X., Guo, J., Chen, T., Li, N., Zhang, F., and Sun, Y.: Revisiting the evolution of downhill thunderstorms over Beijing: a new perspective from a radar wind profiler mesonet, Atmos. Chem. Phys., 24(14), 8067-8083, doi:10.5194/acp-24-8067-2024, 2024.

Guo, X., Guo, J., Zhang, D. L., and Yun, Y.: Vertical divergence profiles as detected by two wind-profiler mesonets over East China: Implications for nowcasting convective storms, Q. J. R. Meteorol. Soc., 149(754), 1629-1649. doi:10.1002/qj.4474, 2023.

Hersbach, H., Bell, B., Berrisford, P., Biavati, G., Horányi, A., Muñoz Sabater, J., Nicolas, J., Peubey, C., Radu, R., Rozum, I., Schepers, D., Simmons, A., Soci, C., Dee, D.and Thépaut, J-N.: ERA5 hourly data on pressure levels from 1940 to present. Copernicus Climate Change Service (C3S) Climate Data Store (CDS), doi: 10.24381/cds.bd0915c6 (Accessed on 06-05-2024), 2023.

Higgins, R. W., Yao, Y., Yarosh, E. S., Janowiak, J. E., and Mo, K. C.: Influence of the Great Plains low-level jet on summertime precipitation and moisture transport over the central United States, J. Clim., 10(3), 481-507, 1997.

Hodges, D., and Pu, Z.: Characteristics and Variations of Low-Level Jets and Environmental Factors Associated with Summer Precipitation Extremes over the Great Plains. J. Clim., 32(16), 5123-5144, doi:10.1175/JCLI-D-18-0553.1, 2019.

Holton, J. R.: The diurnal boundary layer wind oscillation above sloping terrain, Tellus, 19(2), 200-205, doi: 10.3402/tellusa.v19i2.9766, 1967.

Horinouchi, T., Matsumura, S., Ose, T., and Takayabu, Y. N.: Jet-precipitation relation and future change of the mei-yu-baiu rainband and subtropical jet in CMIP5 coupled GCM simulations, J. Clim., 32(8), 2247-2259, doi:10.1175/JCLI-D-18-0426.1, 2019.

Huang, X., Sun, J., and Liu, W.: The interaction between low-level jet evolution and severe convective rainstorms under topographic effect, Acta Meteorol. Sin., 78(4), 551-567, 2020.

https://doi.org/10.5194/egusphere-2025-4939
Preprint. Discussion started: 16 October 2025

Li, N., and Guo, J.: Data for wind profiles associated with LLJs obtained from RWP observations during the warm season (April-October) of 2023-2024 in China [Data set]. Zenodo. https://doi.org/10.5281/zenodo.17176759, 2025.

Li, N., Guo, J., Wu, M., Zhang, F., Guo, X., Sun, Y., Zhang Z., Liang L., Chen T.: Low-level jet and its effect on the onset of summertime nocturnal rainfall in Beijing, Geophys. Res. Lett., 51, e2024GL110840, doi:10.1029/2024GL11084, 2024.

Li, X., and Du, Y.: Statistical relationships between two types of heavy rainfall and low-level jets in South China, J. Clim., 34(21), 8549-8566, doi:10.1175/JCLI-D-21-0121.1, 2021.

Liu, B., Ma, Y., Guo, J. and Wei, G.: Boundary layer heights as derived from ground-based radar wind profiler in Beijing, IEEE Trans. Geosci. Remote Sens., 57, 8095-8104, doi:10.1109/TGRS.2019.2918301, 2019.

Luo, Y., Gong, Y., and Zhang, D. L.: Initiation and organizational modes of an extreme-rain-producing mesoscale convective system along a mei-yu front in East China, Mon. Weather Rev., 142(1), 203-221, doi:10.1175/MWR-D-13-00111.1, 2014.

Maddox, R. A.: Large-scale meteorological conditions associated with midlatitude, mesoscale convective complexes, Mon. Weather Rev., 111(7), 1475-1493, 1983.

Marengo, J. A., Soares, W. R., Saulo, C., and Nicolini, M.: Climatology of the low-level jet east of the Andes as derived from the NCEP-NCAR reanalyses: Characteristics and temporal variability, J. Clim., 17(12), 2261-2280, 2004.

Miao, Y., Guo, J., Liu, S., Wei, W., Zhang, G., Lin, Y., and Zhai, P.: The Climatology of Low-Level Jet in Beijing and Guangzhou, China, J. Geophys. Res. Atmos., 123(5), 2816-2830. doi:10.1002/2017jd027321, 2018.

Mitchell, M. J., Arritt, R. W., and Labas, K.: A climatology of the warm season Great Plains low-level jet using wind profiler observations, Weather Forecast., 10(3), 576-591, 1995.

Molod, A., Salmun, H. and Collow, A.B.M.: Annual cycle of planetary boundary layer heights estimated from wind profiler network data, J. Geophys. Res. Atmos., 124, 6207-6221, doi:10.1029/2018JD030102, 2019.

https://doi.org/10.5194/egusphere-2025-4939
Preprint. Discussion started: 16 October 2025

Monaghan, A. J., Rife, D. L., Pinto, J. O., Davis, C. A., and Hannan, J. R.: Global precipitation extremes associated with diurnally varying low-level jets, J. Clim., 23(19), 5065-5084, 2010.

Pan, H., and Chen, G.: Diurnal variations of precipitation over North China regulated by the mountain-plains solenoid and boundary-layer inertial oscillation, Adv. Atmos. Sci., 36(8), 863-884, doi:10.1175/2010JCLI3515.1, 2019.

Pitchford, K. L., and London, J.: The low-level jet as related to nocturnal thunderstorms over Midwest United States, J. Appl. Meteorol., 1(1), 43-47, 1962.

Rasmussen, K. L., and Houze Jr, R. A.: Convective initiation near the Andes in subtropical South America, Mon. Weather Rev., 144(6), 2351-2374, doi:10.1175/MWR-D-15-0058.1, 2016.

Reif, D. Q., and Bluestein, H.: A 20-year climatology of nocturnal convection initiation over the central and southern great plains during the warm season, Mon. Weather Rev., 145, 1615-1639, doi:10.1175/MWR-D-16-0340.1, 2017.

Roots, M., Sullivan, J. T., and Demoz, B.: Mid-Atlantic nocturnal low-level jet characteristics: a machine learning analysis of radar wind profiles, Atmos. Meas. Tech., 18(5), 1269-1282, doi:10.5194/amt-18-1269-2025, 2025.

Stensrud, D. J.: Importance of low-level jets to climate: A review, J. Clim., 1698-1711, 1996.

Subrahmayam, K. V., Udupa, S. R., Kumar, K. K., Ramana, M. V., Srinivasulu, J., and Bothale, R. V.: Prediction of zonal wind using machine learning algorithms: Implications to future projections of Indian monsoon jets, J. Indian Soc. Remote Sens., 52(2), 371-381, 2024.

Sun, S. Q., Zhai, G. H., and Lorenzo, D. O.: The relationship between large-scale low-level jet over east asia and monsoon as well as cross-equatorial currents in summer, Acta Meteorol. Sin., 1(1), 43-50, 1986.

Trier, J. W. Wilson, D. A. Ahijevych, and R. A. Sobash : Mesoscale vertical motions near nocturnal convection initiation in PECAN, Mon. Weather Rev., 145, 2919-2941, doi:10.1175/MWR-D-17-0005.1, 2017.

https://doi.org/10.5194/egusphere-2025-4939
Preprint. Discussion started: 16 October 2025

Trier, S. B., Davis, C. A., Ahijevych, D. A., Weisman, M. L., and Bryan, G. H.: Mechanisms supporting long-lived episodes of propagating nocturnal convection within a 7-day WRF model simulation, J. Atmos. Sci., 63(10), 2437-2461, doi: 10.1175/JAS3768.1, 2006.

Tuttle, J. D., and Davis, C. A.: Corridors of warm season precipitation in the central United States. Mon. Weather Rev., 134(9), 2297-2317, doi:10.1175/MWR3188.1, 2006.

Walters, C. K., Winkler, J. A., Shadbolt, R. P., van Ravensway, J., and Bierly, G. D.: A long-term climatology of southerly and northerly low-level jets for the central United States, Ann. Assoc. Am. Geogr., 98(3), 521-552, 2008.

Wang, D., Zhang, Y., and Huang, A.: Climatic features of the south-westerly low-level jet over southeast China and its association with precipitation over east China, Asia-Pac. J. Atmos. Sci., 49(3), 259-270, doi:10.1007/s13143-013-0025-y, 2013.

Wang, W. C., Gong, W., and Wei, H.: A regional model simulation of the 1991 severe precipitation event over the Yangtze-Huai River valley. Part I: Precipitation and circulation statistics, J. Clim., 13(1), 74-92, doi:10.1175/1520-0442(2000)013<0074:ARMSOT>2.0.CO;2, 2000.

Weckwerth, T. M., and Wakimoto, R. M.: The initiation and organization of convective cells atop a cold-air outflow boundary, Mon. Weather Rev., 120(10), 2169 – 2187, doi:10.1175/ 1520-0493(1992)120,2169:TIAOOC.2.0.CO;2, 1992.

Weckwerth, T. M., Hanesiak, J., Wilson, J. W., et al.: Nocturnal convection initiation during PECAN 2015, Bull. Am. Meteorol. Soc., 100(11), 2223-2239, doi::10.1175/BAMS-D-18-0299.1, 2019.

Wei, W., Zhang, H. S., and Ye, X. X.: Comparison of low-level jets along the north coast of China in summer, J. Geophys. Res. Atmos., 119(16), 9692-9706. doi:10.1002/2014jd021476, 2014.

Weisman, M. L., Trapp, R. J., Romine, G. S., Davis, C., Torn, R., Baldwin, M., Bosart, L., Brown, J., Coniglio, M., Dowell, D., Evans, A. C., Galarneau, T. J., Haggerty, J., Hock, T., Manning, K., Roebber, P., Romashkin, P., Schumacher, R., Schwartz, C. S., Sobash, R., Stensrud, D., and Trier, S. B.: The mesoscale predictability experiment (MPEX), Bull. Am. Meteorol. Soc., 96(12), 2127-2149, doi:10.1175/bams-d-13-00281.1, 2015.

Whiteman, C. D., Bian, X., and Zhong, S.: Low-level jet climatology from enhanced Rawinsonde observations at a site in the southern Great Plains, J. Appl. Meteorol., 36(10), 1363-1376, doi:10.1175/1520-0450(1997)036%3C1363:LLJCFE%3E2.0. CO;2, 1997.

Xia, R., and Zhao, S.: Diagnosis and modeling of meso-scale systems of heavy rainfall in warm sector ahead of front in South China (middle part of Guangdong province) in June 2005, Chin. J. Atmos. Sci., 33(3), 2009.

Xue, M., Luo, X., Zhu, K., Sun, Z., and Fei, J.: The controlling role of boundary layer inertial oscillations in Meiyu frontal precipitation and its diurnal cycles over China, J. Geophys. Res. Atmos., 123(10), 5090-5115, doi:10.1029/2018JD028368, 2018.

Yan, Y., Cai, X., Wang, X., Miao, Y., and Song, Y.: Low-level jet climatology of China derived from long-term radiosonde observations, J. Geophys. Res. Atmos., 126(20), e2021JD035323, doi:10.1029/2021JD035323, 2021.

Yu, R., Li, J., Chen, H., and Yuan, W.: Progress in studies of the precipitation diurnal variation over contiguous China, J. Meteorol. Res., 28(5), 877-902, doi:10.1007/s13351-014-3272-7, 2014.

Zamora, R.J., Shapiro, M.A. and Doswell, C.A., III.: The diagnosis of upper tropospheric divergence and ageostrophic wind using profiler wind observations, Mon. Weather Rev., 115, 871-884, doi:10.1175/1520-0493(1987)1152.0.CO;2, 1987.

Zhang, F., Zhang, Q., Sun, J., and Xu, J.: Convection initiation during the Meiyu environment in the Yangtze-Huai River basin of China, J. Geophys. Res. Atmos., 128(9), e2022JD038077, doi:10.1029/2022JD038077, 2023.

Zhang, M., and Meng, Z.: Warm-sector heavy rainfall in southern China and its WRF simulation evaluation: A low-level-jet perspective, Mon. Weather Rev., 147(12), 4461-4480, doi:10.1175/MWR-D-19-0110.1, 2019.

Zhang, Y., Xue, M., Zhu, K., and Zhou, B.: What is the main cause of diurnal variation and nocturnal peak of summer precipitation in Sichuan Basin, China? the key role of boundary layer low-level jet inertial oscillations, J. Geophys. Res. Atmos., 124(5), 2643-2664, doi:10.1029/2018jd029834, 2019.

https://doi.org/10.5194/egusphere-2025-4939
Preprint. Discussion started: 16 October 2025

Table 1. Table of Representative Radar Wind Profiler Stations in Mainland China

Region	Station		Longitude (°)	Latitude (°)	Altitude (m)
ROI-1	58839	MQ	118.86	26.22	160.70
	59046	LZ	109.46	24.36	314.40
	59137	JJ	118.54	24.81	124.80
	59287	GZ	113.48	23.21	65.00
	59758	HK	110.25	19.99	69.00
ROI-2	57461	YC	111.36	30.74	253.80
	57687	CS	112.79	28.11	119.00
	57793	YCN	114.36	27.79	132.00
	58238	BJ	118.90	31.93	40.60
	58321	HF	117.03	31.57	50.00
	58367	LH	121.47	31.18	5.00
	58459	XS	120.29	30.18	48.80
ROI-3	53463	HHHT	111.68	40.82	1152.10
	53772	TY	112.58	37.62	785.00
	54511	BJ	116.47	39.81	31.50
	54534	TS	118.10	39.65	23.20
	54602	BD	115.48	38.73	16.80
ROI-4	57816	GY	106.73	26.59	1197.60
	56290	XD	104.18	30.77	514.00
	56651	LJ	100.22	26.85	2382.40
Other stations	50936	BC	122.47	45.36	156.00
	51463	WLMQ	87.65	43.79	935.00
	51628	AKS	80.38	41.12	1107.10
	52754	GC	100.08	37.2	3301.50
	52889	LZ	103.89	36.06	1519.20
	57516	CQ	106.46	29.57	260.00
	53845	YA	109.45	36.58	1180.40
	54342	SY	123.51	41.73	50.00
	54857	QD	120.13	36.23	12.00
	55664	DR	87.07	28.63	4302.00
	57171	PDS	113.12	33.77	142.00

Figures

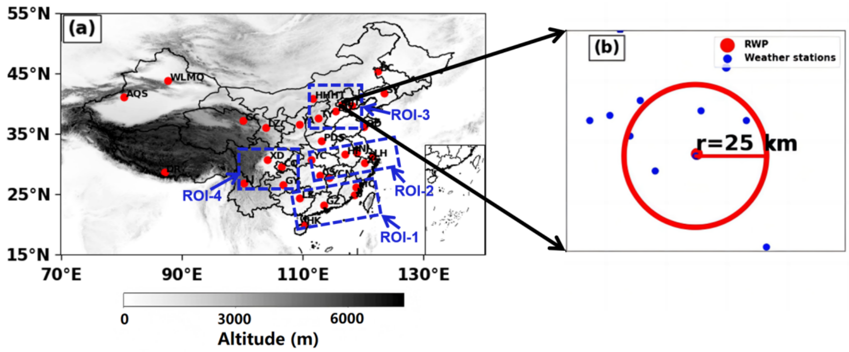

Figure.1 (a) Spatial distribution of 31 Radar Wind Profiler (RWP) stations across China, with four regions of interest (ROIs) demarcated by blue dashed boxes: ROI-1, ROI-2, ROI-3, and ROI-3. (b) Schematic of spatial co-location: Beijing Observatory's RWP (red star) and rain gauges (black dots) within a 25-km radius

https://doi.org/10.5194/egusphere-2025-4939
Preprint. Discussion started: 16 October 2025

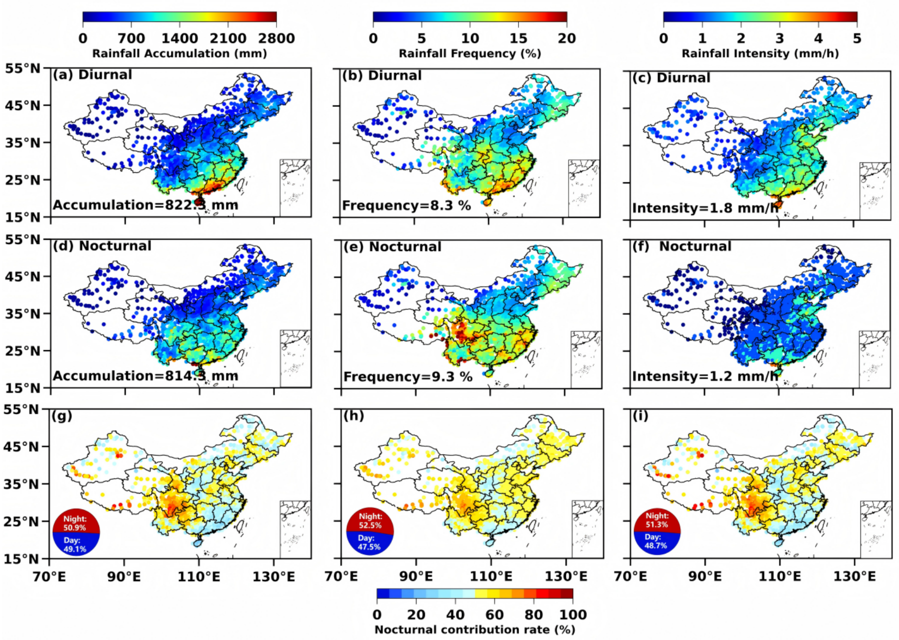

Figure 2. (a–c) Spatial distributions of accumulated rainfall (mm), rainfall frequency (%) and rainfall intensity (mm/h) in the daytime from April to October in 2023–2024. The numbers in the upper left corner represent the national average; (d–f) the same as (a–c), but in the nighttime; (g–i) Nocturnal contribution ratios of accumulated rainfall, frequency, and occurrence frequency of heavy rainfall (>75th percentile intensity). The pie charts illustrate the contribution rates of daytime (blue) and nighttime (red) at the national scale

https://doi.org/10.5194/egusphere-2025-4939
Preprint. Discussion started: 16 October 2025

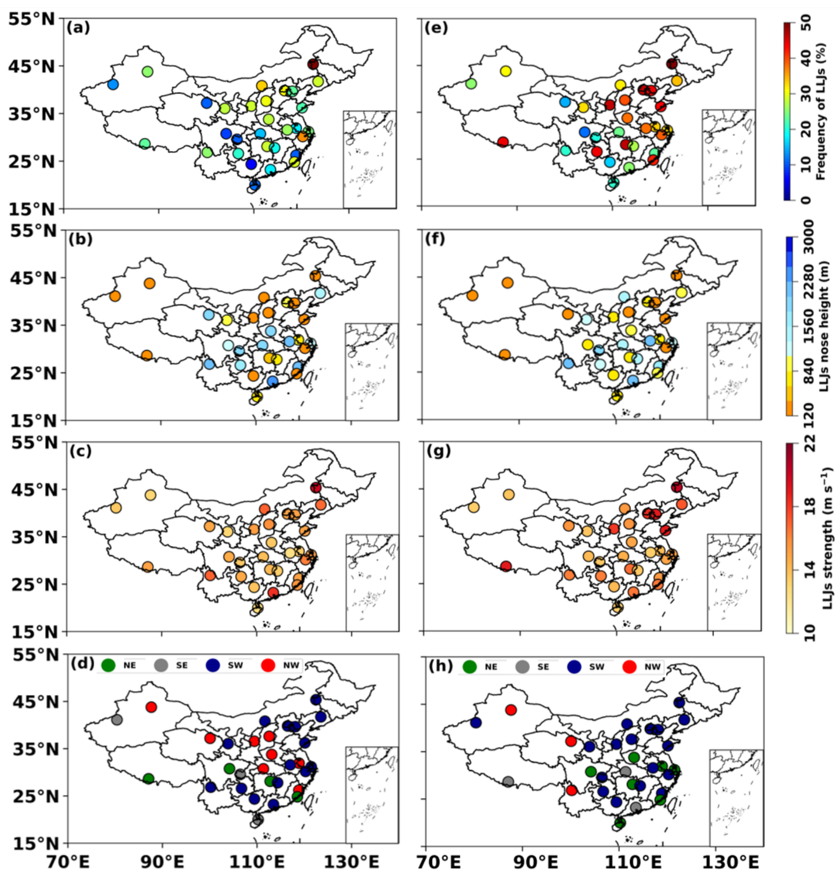

Figure 3. (a–d) Spatial distribution of occurrence frequency, height, strength, and the dominant wind direction of LLJs observed by 31 RWP stations during April-October from 2023 to 2024 in the daytime. (e–h) Same as (a–d), but in the nighttime

https://doi.org/10.5194/egusphere-2025-4939
Preprint. Discussion started: 16 October 2025

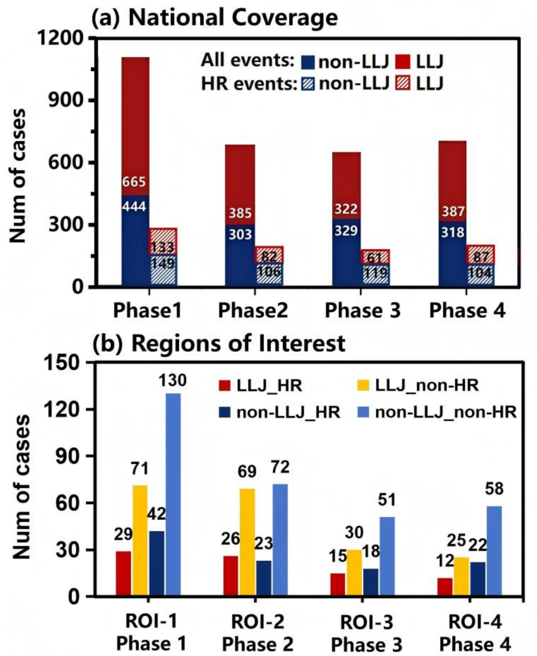

Figure 4. (a) Statistic of all nocturnal rainfall events (solid-filled bars) and heavy rainfall (HR; diagonally striped bars) events selected across China during four phases, including LLJ events (red) and non-LLJ events (blue); (b) Same as panel (a), but for nocturnal HR events in from ROI-1 to ROI-4 during corresponding phase, including LLJ-HR (red), LLJ_non-HR (yellow), non-LLJ_HR (dark blue), and non-LLJ_non-HR (light blue) events.

https://doi.org/10.5194/egusphere-2025-4939
Preprint. Discussion started: 16 October 2025

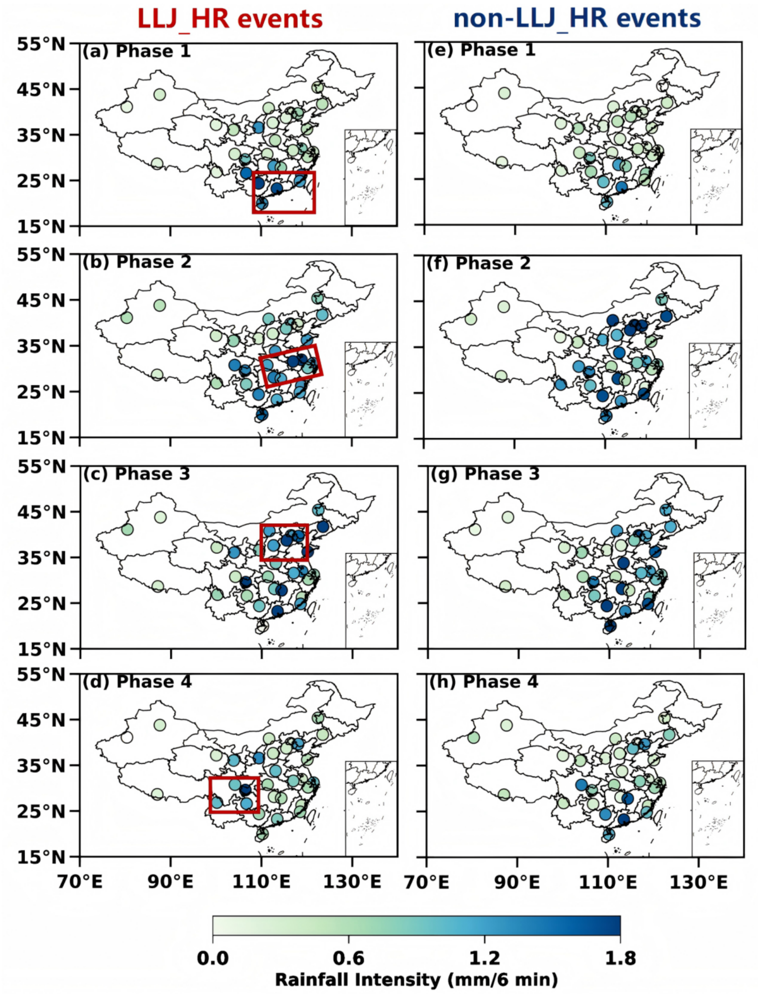

Figure 5. (a–d) Spatial distributions of average rain rate (mm/6 min) for nocturnal LLJ_HR events during the warm season from Phase 1 to Phase 4 across China; (e–h) Same as (a–d), but for non-LLJ_HR events. The red frame indicates four ROIs.

https://doi.org/10.5194/egusphere-2025-4939
Preprint. Discussion started: 16 October 2025

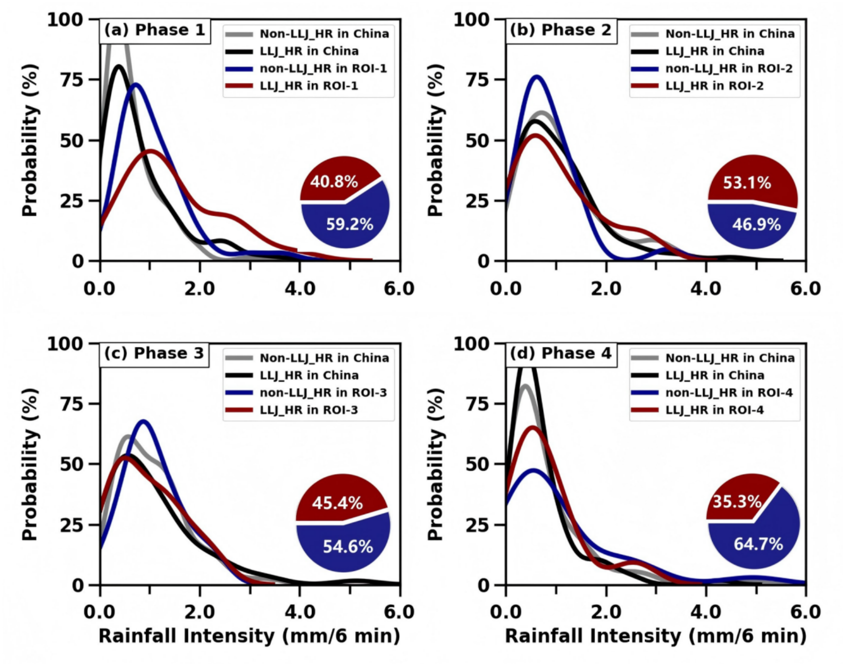

Figure 6. (a) Probability density distributions of average rain rate (mm/6 min) for LLJ-HR events (black solid lines) and non-LLJ_HR events (gray solid lines) across China during Phase 1, and specifically in ROI-1 for LLJ-HR events (red solid lines) and non-LLJ_HR events (blue solid lines). (b-d) the same as panel (a), but for comparisons between national-scale and other regional-scale events in ROI-2 during Phase 2, ROI-3 during Phase 3, and ROI-4 during Phase 4. The pie chart at the lower right shows the proportion distribution of LLJ-HR and non-LLJ_HR events in these key regions during each period

https://doi.org/10.5194/egusphere-2025-4939
Preprint. Discussion started: 16 October 2025

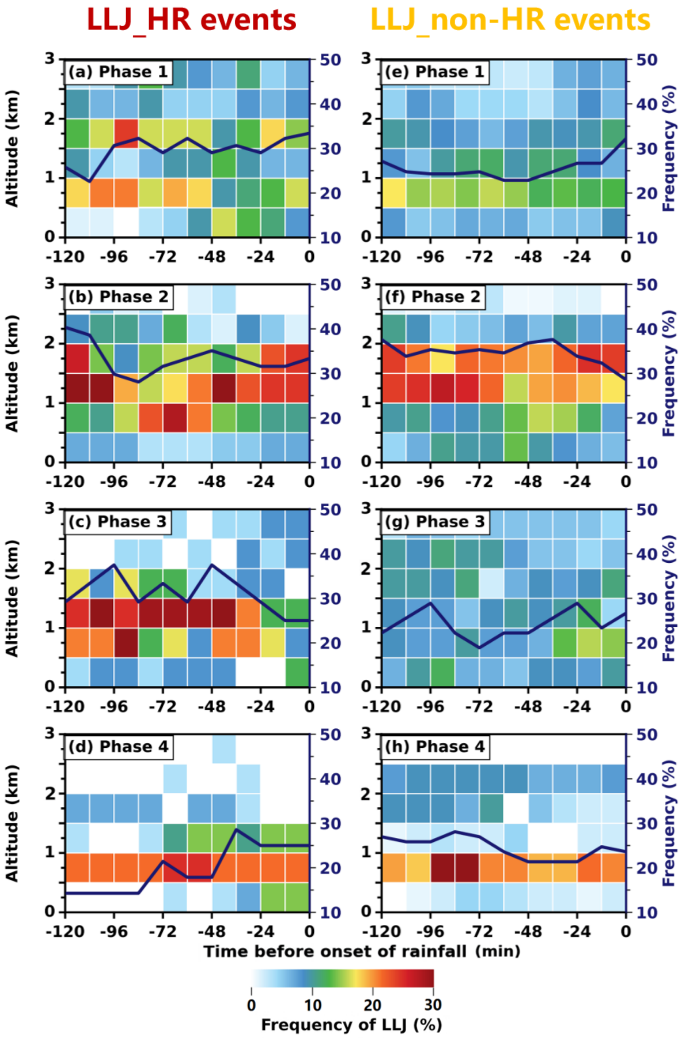

Figure 7. Time-height evolution of LLJ occurrence frequency (color shading, every 12 min, within 500 m vertical bins) detected by RWP with 2 hours preceding nocturnal rainfall in LLJ-HR events in (a) ROI-1 during Phase 1, (b) ROI-2 during Phase 2, (c) ROI-3 during Phase 3, and (d) in ROI-4 during Phase 4. Black solid lines denote accumulated LLJ frequency for 3-km altitude. (e-h) Same as (a-d), but for LLJ_non-HR events

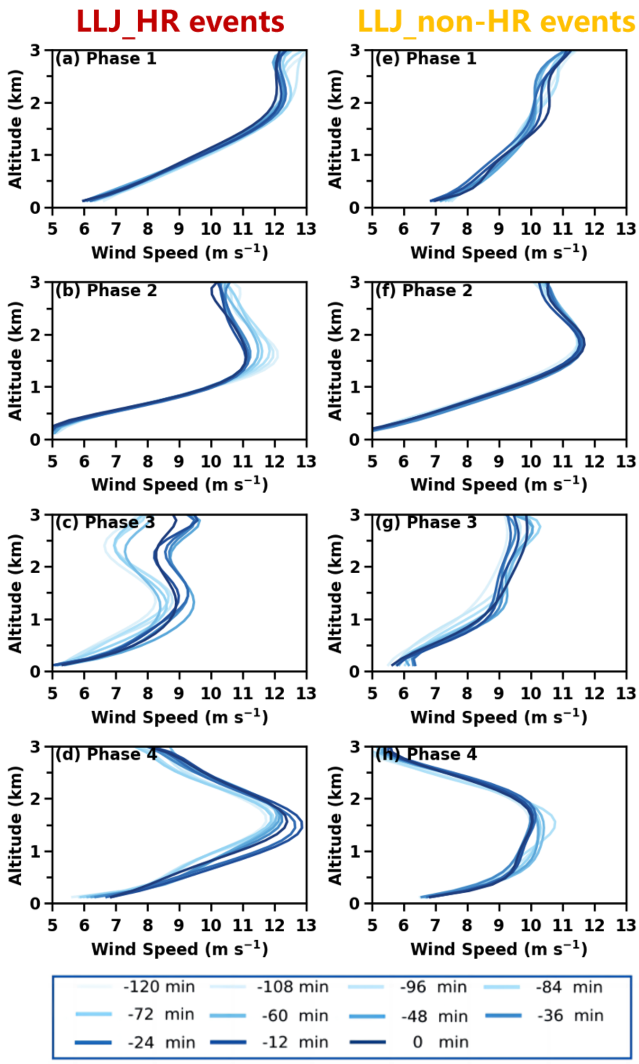

Figure 8. (a-d) Evolution of RWP-detected mean wind profiles of LLJs (blue solid lines, every 12 min) within 2 hours preceding nocturnal rainfall in LLJ-HR events in (a) ROI-1 during Phase 1, (b) ROI-2 during Phase 2, (c) ROI-3 during Phase 3, and (d) in ROI-4 during Phase 4. (e-h) Same as (a-d), but for LLJ_non-HR events

https://doi.org/10.5194/egusphere-2025-4939
Preprint. Discussion started: 16 October 2025

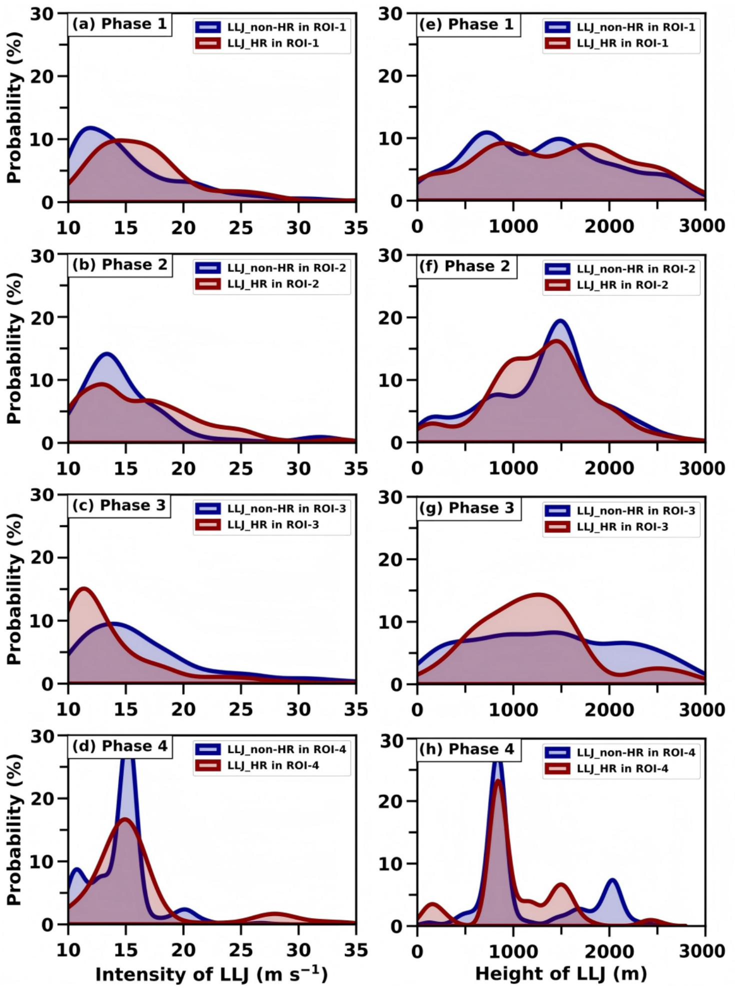

Figure 9. Probability density distributions of jet core intensity from RWP observations within 2 hours preceding nocturnal rainfall in LLJ-HR events in (a) ROI-1 during Phase 1, (b) ROI-2 during Phase 2, (c) ROI-3 during Phase 3, and (d) in ROI-4 during Phase 4. (e-h) Same as (a-d), but for the height of LLJs

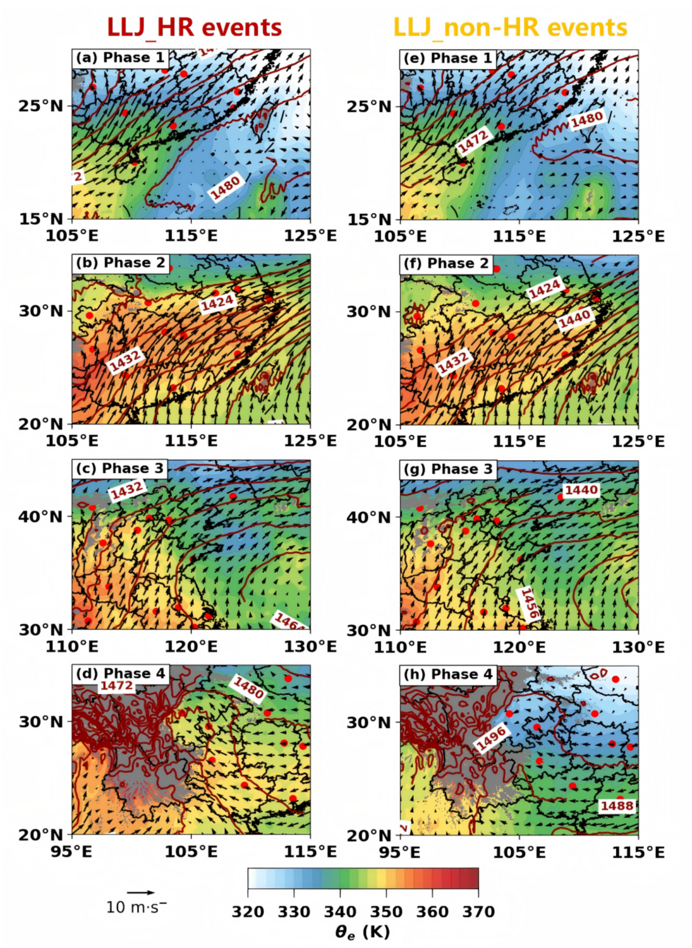

Figure 10. Distributions of equivalent potential temperature (shading, unit: K) at 850 hPa, superimposed with 850 hPa horizontal wind vectors (black arrows) and geopotential height contours (red solid lines), for LLJ-HR events within 1-hour time window preceding nocturnal rainfall onset in (a) ROI-1 during Phase 1, (b) ROI-2 during Phase 2, (c) ROI-3 during Phase 3, and (d) in ROI-4 during Phase 4. Gray shading denotes terrain elevation exceeding 850 Pa level. The reference vector (10 m s^{-1}) is shown at the lower-left corner. (e-h) Same as (a-d), but for LLJ_non-HR events

https://doi.org/10.5194/egusphere-2025-4939
Preprint. Discussion started: 16 October 2025

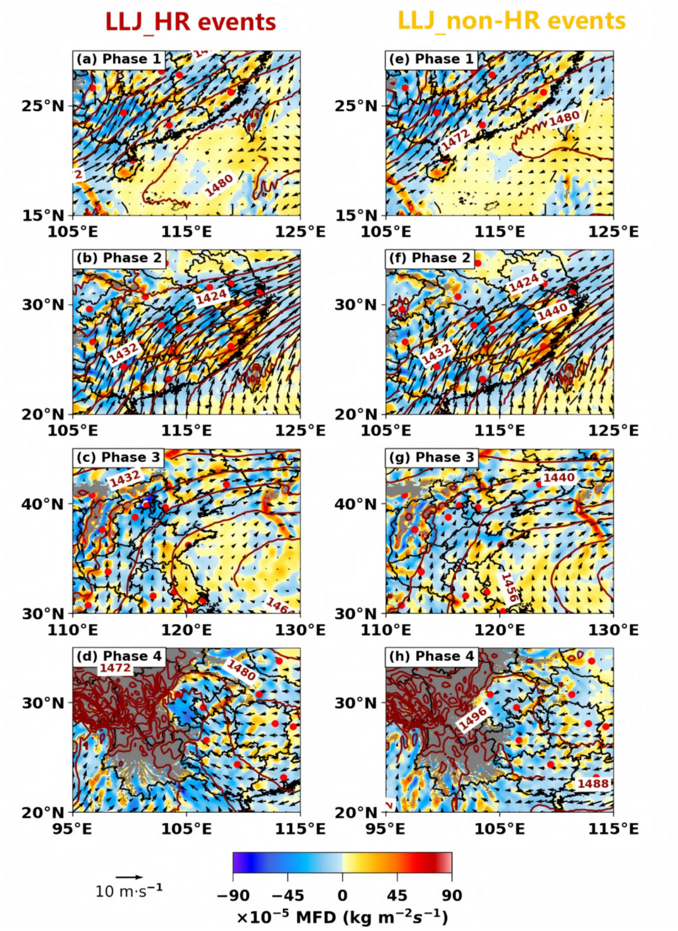

Figure 11. Same as Figure 10, but showing the integrated moisture flux divergence (shading, unit: kg·m^{-2} s^{-1}) between 1000–700 hPa at 1 hour preceding nocturnal rainfall onset

https://doi.org/10.5194/egusphere-2025-4939
Preprint. Discussion started: 16 October 2025

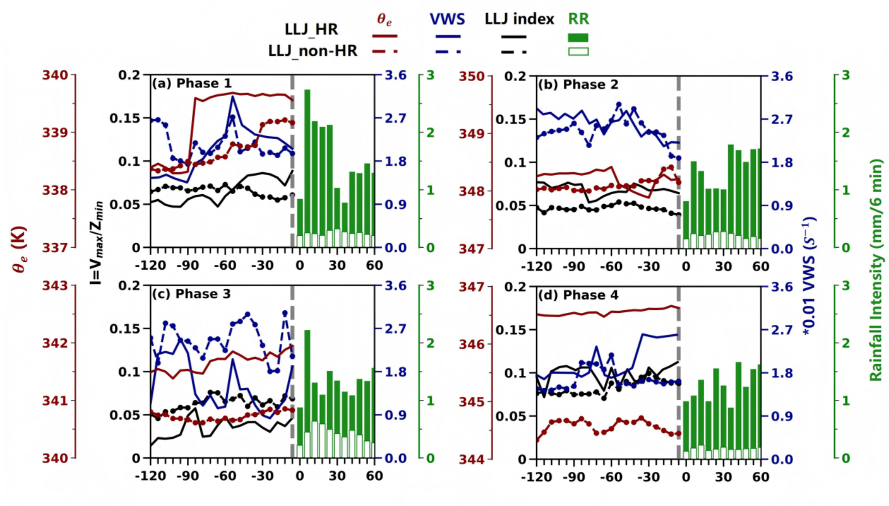

Figure 12. Temporal evolution of surface equivalent potential temperature (θ_e, red lines), vertical wind shear (VWS, blue lines), and LLJ index (I, black lines) averaged within 2 hours preceding nocturnal rainfall for LLJ-HR events (solid lines) and LLJ_non-HR events (dashed lines) in (a) ROI-1 during Phase 1, (b) ROI-2 during Phase 2, (c) ROI-3 during Phase 3, and (d) in ROI-4 during Phase 4. Green bars denote 6-min averaged rain rate (mm/ 6 min) after LLJ-HR (solid bars) and LLJ_non-HR (open bars) events onset